Research Article

Wahyu Meka, Orchidea Rachmaniah*, Rijalul Mulhim Al-Mauhub, Nathanael Abishai Widiraga, Ratri Safira Tirta Afida, Patricia Evangeline Toqueville Purba, Latifa Hanum Lalasari, Anugerah Dany Priyanto, Henni Vanda, Mahardika Fahrudin Rois, Yulia Fitri, and Salman Masoudi Soltani

Production of liquid smoke by consecutive electroporation and microwave-assisted pyrolysis of empty fruit bunches

https://doi.org/10.1515/gps-2025-0022 received January 26, 2025; accepted August 05, 2025

Abstract: This study investigated the combined effects of electroporation and microwave-assisted pyrolysis (MAP) on the characteristics of liquid smoke produced from empty fruit bunches (EFBs). Ground EFBs were subjected to electroporation in an electroporation chamber at varying electric fields of 15 and 20 kV·cm⁻¹ and subsequently pyrolysed at varying temperatures of 300°C and 400°C in a modified microwave oven connected to a condensation system. Electroporation significantly altered EFB structure, with higher electric fields (20 kV·cm⁻¹) causing greater structural disruptions, as evidenced by reduced pore sizes. MAP of EFBs electroporated at 15 kV·cm⁻¹ produced a higher liquid smoke yield, while severe electroporation (20 kV·cm⁻¹) resulted in lower yields but higher antioxidant capacity and lower pH. This was attributed to improved chemical selectivity under

high electric fields and phenolic enrichment. A proposed lignocellulose degradation mechanism outlined the roles of MAP temperature and electric fields in influencing chemical conversion pathways. These findings highlight the potential for optimising electroporation and MAP to enhance the valorisation of EFBs, providing a sustainable green approach for producing high-quality liquid smoke from agricultural waste.

Keywords: agricultural waste, electroporation, liquid smoke, microwave, pyrolysis

1 Introduction

Since the beginning of the twenty-first century, global circumstances of climate change, healthy lifestyle, animal prosperity, and environmental issues have promoted an increase in green consumption behaviour, such as the consumption of organic food that is free from unhealthy synthetic chemical compounds [1,2]. Despite benefits to human health and environment, organic food undergoes rapid chemical and biological decomposition due to the absence of preservatives. In other words, organic food production requires allocating more resources than nonorganic food production to compensate loss due to quick deterioration during the process [3]. Hence, the application of organic preservatives is imperative to overcome such problems.

Liquid smoke, also known as wood vinegar, is one of the most common food preservatives. Since originating from wood, liquid smoke is considered natural and suitable for human consumption as a food additive. In addition, due to its specific chemical compositions, liquid smoke has functionality as a flavouring agent and a healthy source of bioactive compounds [4,5]. As estimated by Research and Markets, liquid smoke is forecasted to have promising opportunities as a food preservative with an estimated market size of USD0.2 billion by 2030 [6].

Wahyu Meka, Rijalul Mulhim Al-Mauhub, Nathanael Abishai Widiraga, Ratri Safira Tirta Afida, Patricia Evangeline Toqueville Purba: Department of Chemical Engineering, Institut Teknologi Sepuluh Nopember, Surabaya, Indonesia

Latifa Hanum Lalasari: Research Center for Metallurgy, National Research and Innovation Agency, Tangerang Selatan, Indonesia Anugerah Dany Priyanto: Department of Food Technology, Faculty of Engineering, Universitas Pembangunan Nasional Veteran Jawa Timur, Surabaya, Indonesia

Henni Vanda: Faculty of Veterinary Medicine, Universitas Syiah Kuala, Banda Aceh, Indonesia

Mahardika Fahrudin Rois: Research Center for Advanced Material, National Research and Innovation Agency, Tangerang Selatan, Indonesia Yulia Fitri: Faculty of Mathematics, Natural Science, and Health, Universitas Muhammadiyah Riau, Pekanbaru, Indonesia Salman Masoudi Soltani: Department of Chemical Engineering, Brunel

University of London, Uxbridge, UB8 3PH, United Kingdom

^{*} Corresponding author: Orchidea Rachmaniah, Department of Chemical Engineering, Institut Teknologi Sepuluh Nopember, Surabaya, Indonesia, e-mail: orchidea@its.ac.id

Despite predominance as a liquid smoke source, wood is less favoured to exploit since wood consumption allows forest logging that causes negative consequences on forest ecosystems, e.g., reduced biodiversity, land erosion, and contaminated watershed [9]. Furthermore, deforestation is one of the primary causes of global warming [10]. Thus, the substitution of wood at this stage is of great importance.

Empty fruit bunches (EFBs) of oil palm are a potential substitute for wood as a raw material for liquid smoke. They are extremely abundant waste, annual production of which reaches approximately 74–99 tons in Indonesia and Malaysia combined [11,12]. Unfortunately, only a small fraction of these copious EFBs is valorised, whereas the remaining are left to rot due to anaerobic degradation that potentially produces methane, promoting global warming [13]. More importantly, as lignocellulosic materials, both EFBs and wood share similar chemical compositions of cellulose, hemicellulose, and lignin [14].

Thermal degradation of EFBs via pyrolysis has been intensively researched [15–26]. Many experiments of thermal degradation of EFBs were previously conducted, most of which, however, were performed to obtain biofuel as an alternative energy, whereas only a tiny fraction was intended for liquid smoke production. Despite having identical production techniques, liquid smoke and biofuel are disparate and produced in, respectively, unique operating conditions, e.g., pyrolysis reactor types.

Kilns and fluidised beds are conventional reactor types commonly used in liquid smoke production via pyrolysis. Kilns pyrolyse a large volume of biomass and have simple operability. However, high liquid product yield is onerous to achieve due to very slow heating rates [27]. Fluidised beds feature higher heating rates that induce higher liquid product yield compared to kilns [28]. Nevertheless, fluidised beds are rigorous to use and scale up due to their process operation intricacy [29].

Reactors with microwave assistance are one of the most advanced devices for pyrolysis due to their advantages. The reactors use microwaves to perform dipolar rotation on water and any other polar chemical compounds within the biomass. Molecular friction occurring due to dipolar rotation engenders the generation of heat

that increases biomass temperatures and eventually thermally degrades the biomass. This entire mechanism is superbly efficient since heat generation via relatively slower convection and conduction is absent [30]. In addition, microwave application requires no physical contact between heated materials and magnetrons, which eliminates potential contamination to the heated materials [31]. Despite the advantages, reactors with microwave assistance remain nascent; hence, future optimisation development is expected for commercial-scale realisation.

Electroporation as pretreatment is one of the most potential pyrolysis optimisation techniques. It is high-voltage-induced pulsed electrocution of biomass that aims either to improve biomass porosity and permeability or to extract certain precious organic compounds via cell membrane disruption, followed by intracellular fluid removal [32,33]. The enhanced porosity and permeability consequently boost transport properties of the biomass, e.g., rates of heat and mass diffusion into and out of the biomass. Another electroporation advantage is post-electrocution chemically intact structures of lignocellulose since electroporation is applied at room temperatures; Thus, chemical degradation producing unexpected lignocellulose-derived chemical compounds that potentially interfere with the subsequent treatment performance and final product quality is not anticipated.

The effects of the electroporation-boosted transport properties of biomass on subsequent treatments, such as enzymatic hydrolysis, conversion to biogas, mechanical extraction, and combustion, have been previously examined. The porosity of switchgrass and wood chips was significantly increased through electroporation using a pulsed electric field (PEF) at electric field strengths exceeding 8 kV·cm⁻¹. This enhancement was reported to improve cellulose exposure, thereby facilitating more efficient conversion of cellulose into fuels or chemicals [34]. Similarly, increasing the porosity of maize silage substrate was theorised to enhance its biogas production efficiency [35]. This hypothesis was later confirmed, revealing a clear link between increased biogas yield and the reduction in lignocellulose content as the duration of electroporation increased [36]. In the case of seaweed, electroporation also improved porosity, which in turn doubled the efficiency of ash removal during subsequent processing [37]. Furthermore, PEF-induced electroporation alters the internal structure of wood-based materials, making them more porous. This structural change is believed to result in faster ignition, more efficient combustion, and altered combustion temperatures [38]. However, later findings indicated that while PEF treatment does not increase the total heat released during wood combustion, it does affect the rate and timing of heat release throughout the burning process [39].

However, such effects on EFB MAP performance, particularly the quality of the produced liquid smoke, have never been investigated and are still not well understood. Hypothetically, based on the previously mentioned literature, high electric field application to EFBs would induce significant intracellular water removal, which could potentially reduce liquid smoke yield but increase antioxidant capacity and reduce the acidity of the liquid smoke. On the other hand, the effect of microwaves on electroporated EFBs would synergistically enhance heating rates, which could adversely affect the antioxidant capacity of the liquid smoke due to the secondary cracking of phenolic compounds at low temperatures. Hence, this article aims to explore the potential of consecutive treatment of electroporation and MAP of EFBs as a novel approach for liquid smoke production by examining how this work aligns with the described hypothesis and addresses the possible mechanisms.

2 Materials and methods

2.1 Raw material preparation

The EFBs were cultivated in oil palm plantations in East Kotawaringin, Central Kalimantan, and provided by Agro Indomas (a private company engaged in oil palm plantations and crude palm oil production). Before any treatment, the EFBs were ground to small particles sized below 60 mesh to increase the EFBs' surface areas and consequently improve rates of heat and mass transfer during electroporation and pyrolysis. Commercial activated carbon having roughly a 2-mm particle size was mixed with the ground EFBs to assist microwave absorption during pyrolysis.

2.2 Raw material analysis

Proximate analysis (% a.r.) and ultimate analysis (% d.a.f.) were conducted on the EFBs according to ASTM D3180-15 and ASTM D-5373-16, respectively. Physical analysis of scanning electron microscopy (SEM) and Brunauer-Emmett-Teller (BET) with N₂ was conducted on the EFBs prior and after electroporation. The equipment used was Phenom P-series by Thermo Fisher Scientific, Luxor^{Au} by Luxor, and NOVAtouch LX4 by Anton Paar for SEM, EFB coating, and BET, respectively. Before SEM analysis, the sample of EFBs was coated with gold to prevent electron absorption by the sample during analysis. After coating, the sample was put into the sample chamber and kept for around 20 min while the power gradually increased. Once ready, the secondary electron was beamed three times at the same position on the sample with varying enlargement. The backscattered electron was then beamed with a similar technique. For BET analysis, the sample was initially stored in a desiccator at low temperature to minimise water content and then degassed for an hour at a constant temperature of 105°C to remove gas content prior to BET analysis.

2.3 Experimental setup and procedure

A laboratory-scale electroporation system used for EFB electroporation was customised according to Figure 1(a). The electroporation system, featuring a frequency of 8.197 kHz and a pulse of 66 µs, consisted of an electroporation chamber (number 1) and a control box (number 8). The electroporation chamber was a stainless-steel cylinder with a volume of 1.51 and diameter-to-height ratio of 0.5. An agitator comprised of an agitator rod (number 4) and agitator blades (number 5) was installed at the electroporation chamber centreline and rotated using an agitator motor (number 7). The electroporation chamber was also equipped with two cathode plates (number 2) and an open-ended cylindrical anode (number 3), which made a concentric radial structure with the electroporation chamber. The distance between the anode and the inner curved surface of the electroporation chamber was 3.65 cm, whereas that between the cathode and the outer curved surface of the electroporation chamber was less than 1 cm. The agitator motor power and the voltage between the cathode and the anode were supplied by the control box through cables (numbers 13, 14, and 15). Several configurable parameters were shown on the control box, namely, temperatures, angular velocities of the agitator, time, and input voltages.

The electroporation was conducted with the following orderly procedure: electrocution, filtration, and drying. Before running the electroporation system, initially, EFBs were mixed with demineralised water with a concentration of 100 mg of EFBs in 700 ml of demineralised water. This slurry mixture was put into the electroporation chamber (number 1) and stirred using the agitator (numbers 4 and 5) at a fixed angular velocity of 48.21 rpm for roughly 5 min. After 5-min agitation, the slurry mixture was electrocuted for roughly 10 min by generating the

electric fields of 15 and 20 kV·cm⁻¹. These electric fields were achieved by adjusting the input voltage according to the empirical relationship shown in Figure 1(b). After electrocution, the slurry was put into a vacuum-pump-assisted filtration apparatus to separate the EFB from the water. The EFBs were later stored in an oven set at 90°C for 12-h drying before MAP.

The laboratory-scale MAP system shown in Figure 1(c) consisted of a customised microwave oven (number 1) and a control box (number 13). The microwave oven was an Electrolux EMM20K22BA, which had five power levels: Melt (136 W), Defrost (264 W), Simmer (440 W), Reheat (616 W), and Quick Cook (800 W). The top of the microwave oven was holed to allow placement of a three-neck round-bottom flask (number 2) whose left, middle, and right necks were connected to the inlet of a Liebig condenser (number 3), cylinder of N_2 (number 9) via plastic hose

(number 10), and thermocouple probe (number 11), respectively. Temperature measured by the ceramic-coated thermocouple probe was sent as signals (number 12) to the control box (number 13) and consequently corrected by sending a correction signal (number 16) back to the microwave oven to regulate microwave generation from the magnetron. During condensation, water as a cooling medium steadily flows from Liebig condenser annulus inlet (number 5) to Liebig condenser annulus outlet (number 4). The outlet of the Liebig condenser (number 2) was connected to the middle neck of another three-neck round-bottom flask (number 6). The right neck of this three-neck round-bottom flask was completely plugged, whereas the left neck was used to remove gas via a plastic hose (number 7) out of the system (number 8).

The MAP procedure was preheating followed by pyrolysis at 300°C and 400°C. Once the well-mixed mixture of

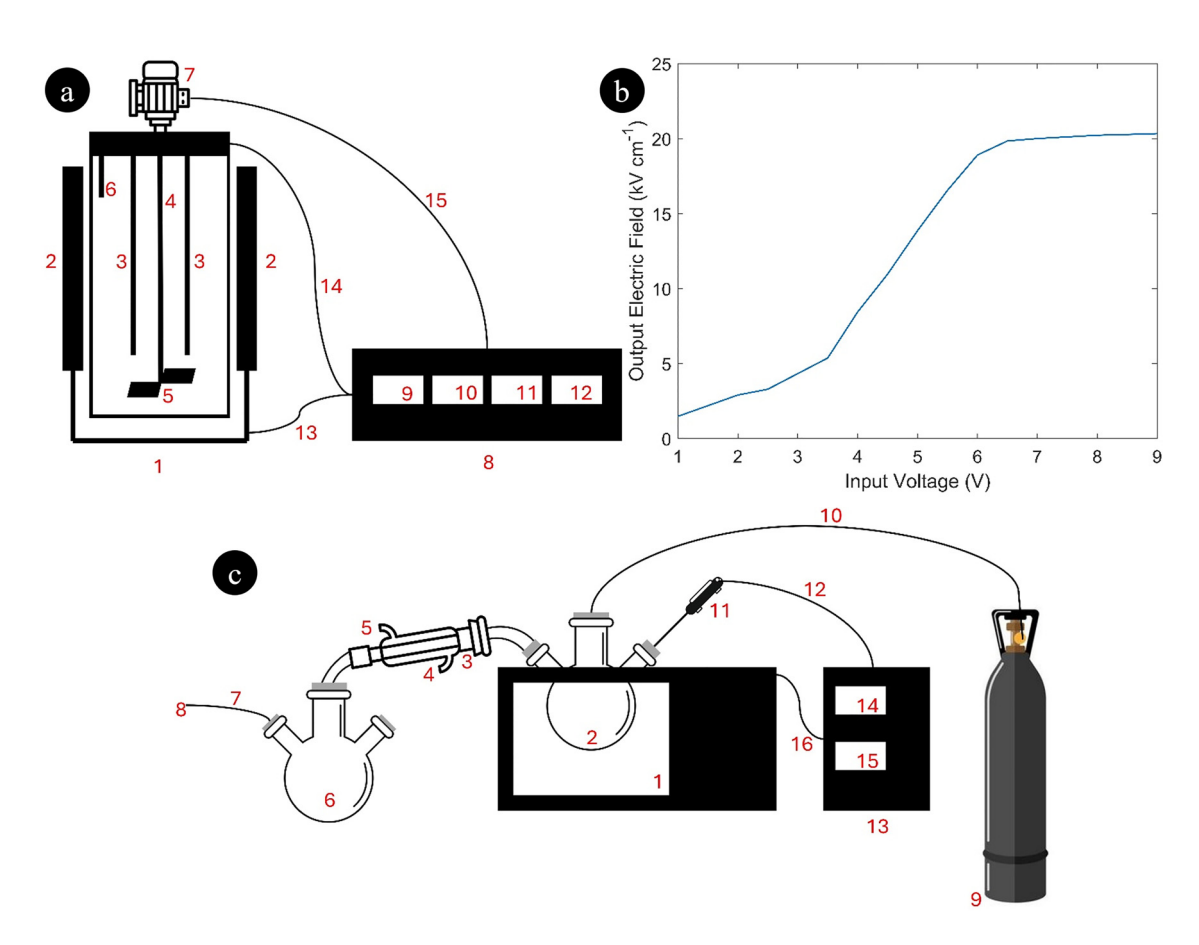


Figure 1: (a) Experimental setup of electroporation: 1, electroporation chamber; 2, cathode; 3, anode; 4, agitator rod; 5, agitator blades; 6, temperature sensor; 7, agitator motor; 8, control box; 9, temperature display; 10, display of angular velocity of agitator; 11, timer display; 12, input voltage display; 13, electrical cable; 14, electrical cable; 15, electrical cable, (b) electric field calibration curve in electroporation system, (c) experimental setup of microwave-assisted pyrolysis (MAP): 1, microwave oven; 2, three-neck round-bottom flask; 3, Liebig condenser; 4, Liebig condenser annulus outlet; 5, Liebig condenser annulus inlet; 6, three-neck round-bottom flask to collect liquid products; 7, plastic hose; 8, outlet flow of non-condensable gas; 9 cylinder of nitrogen; 10, plastic hose; 11, thermocouple probe; 12, electrical cable; 13, control box; 14, temperature display; 15, wattage display; 16, electrical cable.

EFBs and activated carbon at ratio of 9 to 1 was put into the former three-neck round-bottom flask (number 2), the N₂ was released for roughly 5 min from the cylinder at 0.01 l·min⁻¹ to purge air and establish an oxygen-free environment in the flask (number 2). The flask (number 2) was then heated to 100°C by setting the temperature setpoint on the control box and the power level at Melt for approximately 5 min. After 100°C had been achieved, both the temperature setpoint and power level were raised to pyrolysis temperatures and simmered in less than a minute, respectively. Once the pyrolysis temperatures were maintained, the EFB pyrolysis was allowed to occur for roughly 3 to 4 min. During pyrolysis, the liquid product formed due to condensable gas condensation in the Liebig condenser was collected in the latter three-neck round-bottom flask, while the gas product of non-condensable gas was released from the system (number 8). The collected liquid product was then treated in a centrifuge (Ruicheng MC6000) at 6,000 rpm to separate the liquid smoke (light phase) from the carcinogenic-compound-rich heavy phase. The MAP procedure for each temperature and electric field strength was replicated three times. Three measured yields of pyrolytic products, e.g., liquid smoke, tar, char, and gas, for each temperature and electric field strength were measured and used to calculate the mean and standard deviation.

2.4 Liquid smoke analysis

Chemical compound, total phenolic content (TPC), antioxidant capacity, and pH analysis were conducted on the liquid smoke. Agilent 7890B Gas Chromatography was used for the identification of chemical compounds commonly found in liquid smoke, e.g., phenolic compounds, furanic compounds, carbonyl-containing compounds, and carboxylic acids. The TPC was analysed via the gallic acid equivalence method that utilises Folin-Ciocâlteu reagent. Antioxidant capacity was measured via 1,1-diphenyl-2-picrylhydrazyl (DPPH) assay. In the antioxidant capacity analysis, UV-Vis spectrophotometer was used to measure chromogen colour change of DPPH-added liquid smoke due to DPPH neutralisation expressed with EC50 or antioxidant concentrations required for DPPH neutralisation, causing a decrease of DPPH absorbance level by 50%. The pH was measured using a Hanna Instrument HI981030 pH meter.

2.4.1 Chemical compound analysis

Chemical compound analysis of liquid smoke was performed using Gas Chromatography-Mass Spectrometry (GC-MS), following a procedure described elsewhere [40] with several modifications. Prior to analysis, 1 ml of the liquid smoke sample was mixed with 2 ml of analytical-grade dichloromethane, purchased from Sigma-Aldrich. The mixture was sonicated for approximately 5 min to ensure the formation of two clearly separated phases: an aqueous phase (upper layer) and a dichloromethane phase (lower layer). One ml of the lower phase was diluted with analytical-grade dichloromethane to prepare a 5 ml solution for injection into the GC-MS system. Prior to injection, anhydrous sodium sulphate was added to the sample solution, which was then syringefiltered to minimise water content.

An Agilent 7890B gas chromatograph coupled with a 5977B mass spectrometer detector and equipped with an HP-5MS UI column (30 m \times 250 μ m \times 0.25 μ m) was used for the analysis. A 1 µl injection volume was introduced with a split ratio of 10:1, and the injection temperature was set to 270°C. The oven temperature program began at 40°C (held for 5 min), increased to 100°C at a rate of 5°C·min⁻¹, and then to 280°C at a rate of 4°C·min⁻¹, where it was held for 3 min. Helium gas was used as the carrier at a flow rate of 1.2 ml·min⁻¹. Mass spectra were obtained in electron ionisation mode at 70 eV, with an acquisition range of 50-600 amu. Chemical compound identification was performed by comparing the mass spectra with those in the NIST Research Library database (Agilent Technologies) and previous studies [40-42]. Mass spectra with a quality (MSQ) score of ≥85% were considered reliably identified, while those with scores below 80% were classified as impurities. A comparative assessment of the approximate purity of the liquid smoke products was performed using total sum normalisation (TSN). TSN is a widely used and straightforward method for normalising GC-MS data [43], expressing the results as relative [43,44] or semi-quantitative concentrations [45]. This approach is particularly suitable for screening purposes in the absence of standard calibration [43,44] and when quantification is impractical due to the large number of identified compounds (Table 1) [45]. In this study, TSN was applied to illustrate overall compositional trends rather than to quantify absolute concentrations [43-45]. The method involves dividing the area of each individual peak by the total peak area within the same chromatographic profile [43]. Peaks marked as "n.d." (not detected) in Table 1 refer to compounds that were undetected in a particular sample but were present in at least one other sample analysed using the same method.

2.4.2 TPC analysis

The phenolic content was measured using TPC analysis with the Folin-Ciocâlteu reagent and expressed as

equivalent concentrations of gallic acid. A calibration curve was prepared prior to the analysis. A standard solution was prepared by dissolving 3 mg of gallic acid in methanol to create a 10 ml primary solution. To construct the calibration curve, a series of gallic acid solutions with

varying concentrations (e.g., six different concentrations) were prepared by diluting the primary solution. For each concentration, 200 μl of the gallic acid solution was mixed with 1.5 ml of 10% (w/w) Folin–Ciocâlteu reagent. These mixtures were stored in a dark compartment to prevent

Table 1: GC-MS-measured normalised mass percentage of chemical compounds in liquid smoke

Chemical compounds (ID)	Normalised mass percentage					
	300°C			400°C		
	0 kV·cm ^{−1}	15 kV·cm ^{−1}	20 kV·cm ⁻¹	0 kV·cm ^{−1}	15 kV·cm ^{−1}	20 kV·cm ^{−1}
Phenolic compounds						
Phenol (P1)	40.69	44.41	31.07	31.15	33.57	20.56
2-Methoxyphenol or guaiacol (P2)	7.65	7.39	6.03	7.85	6.35	4,00
4-Ethyl-2-methoxyphenol (P3)	n.d.	1.12	0.53	0.66	0.74	n.d.
2-Methoxy-4-vinylphenol (P4)	n.d.	n.d.	0.87	0.63	n.d.	n.d.
2-Methoxy-5-methylphenol (P5)	0.56	n.d.	0.48	n.d.	0.68	n.d.
2,6-Dimethoxyphenol or syringol (P6)	7.44	6.93	3.66	11.24	5.85	4.90
3,5-Dimethoxy-4-hydroxytoluene (P7)	0.46	0.64	n.d.	0.89	0.66	n.d.
4-Ethenyl-2,6-dimethoxyphenol (P8)	n.d.	n.d.	n.d.	0.63	n.d.	n.d.
4-Propenyl-2,6-dimethoxyphenol (P9)	n.d.	n.d.	n.d.	0.47	n.d.	n.d.
Creosol (P10)	n.d.	n.d.	n.d.	0.71	n.d.	n.d.
Catechol (P11)	n.d.	n.d.	n.d.	1.17	n.d.	n.d.
3-Methoxy-1,2-benzenediol (P12)	n.d.	n.d.	n.d.	2.26	0.91	0.98
3-Methyl-1,2-benzenediol (P13)	n.d.	n.d.	n.d.	0.41	n.d.	n.d.
Syringylacetone (P14)	n.d.	n.d.	n.d.	1.55	0.76	1.20
4-Butylguaiacol (P15)	n.d.	n.d.	n.d.	0.97	0.38	n.d.
1-methylnaphthalene (P16)	n.d.	1.06	n.d.	n.d.	n.d.	n.d.
Diester phthalic acid (P17)	12.14	n.d.	n.d.	n.d.	n.d.	n.d.
Subtotal	68.94	61.56	42.64	60.59	49.89	32.49
Carbonyl-containing compounds						
2-Methyl-2-cyclopentenone (CC1)	n.d.	n.d.	0.53	1.38	0.79	n.d.
2-Hydroxy-3-methyl-2- cyclopentenone (CC2)	n.d.	n.d.	n.d.	4.05	n.d.	n.d.
3-Hydroxy-2-methyl-2-cyclopentenone (CC3)	2.07	n.d.	1.07	n.d.	1.91	1.61
3-Ethyl-2-hydroxy-2-cyclopentenone (CC4)	0,77	n.d.	n.d.	1.37	0.62	n.d.
Methyl ester hexadecenoic acid (CC5)	1.31	n.d.	n.d.	n.d.	n.d.	n.d.
2,4-Dimethyl-1,3-cyclopentanedione (CC6)	n.d.	n.d.	n.d.	0.34	n.d.	n.d.
3,5-Dimethoxy-4-hydroxyacetophenone (CC7)	n.d.	n.d.	n.d.	0.54	n.d.	n.d.
4-Hydroxy-3-methoxyphenylacetone (CC8)	n.d.	n.d.	n.d.	n.d.	n.d.	0.61
Subtotal	4.15	n.d.	1.6	7.68	3.32	2.22
Furanic compounds	4.13	11.4.	1.0	7.00	3.32	
3-Furaldehyde (F1)	n.d.	n.d.	4.7	n.d.	n.d.	n.d.
2-Acetylfuran (F2)	n.d.	n.d.	n.d.	0.60	n.d.	n.d.
3-Methylfuran (F3)	n.d.	n.d.	n.d.	n.d.	1.16	n.d.
Subtotal	n.d.	n.d.	4.7	0.6	1.16	n.d.
Nitrogeneous compounds	ii.u.	ii.u.	7.7	0.0	1.10	II.u.
3-Pyridinepropionic acid	n.d.	n.d.	n.d.	0.81	n.d.	n.d.
Subtotal	n.d.	n.d.	n.d.	0.81	n.d.	n.d.
Miscellaneous compounds	ii.u.	ii.u.	n.u.	J.01	ii.u.	ii.u.
1,2,3-Trimethoxy-5-methylbenzene	n.d.	n.d.	n.d.	0.99	0.81	0.66
Subtotal	n.a. n.d.	n.a. n.d.	n.a. n.d.	0.99 0.99	0.81 0.81	0.66
	II.u.	II.u.	II.u.	0.33	U.O I	0.00
Impurities (I)	26.91	20 11	E1 06	20.22	44.82	64.62
Impurities (I)		38.44	51.06 51.06	29.32		
Subtotal	26.91	38.44	51.06	29.32	44.82	64.62

Bold values are used to emphasise the total mass percentage of each chemical compound group. n.d., not detected.

light exposure for 5 min. Next, $1.5 \, \text{ml}$ of 5% (w/w) $\text{Na}_2 \text{CO}_3$ solution was added, and the mixtures were returned to the dark compartment for 2 h. Finally, the absorbance of each mixture was measured with a spectrophotometer at a wavelength of 750 nm, with each measurement repeated three times.

For TPC analysis of the liquid smoke samples, a liquid smoke solution was prepared by dissolving 1 mg of liquid smoke in 1 ml of methanol. A 200- μ l aliquot of this solution was combined with 1.5 ml of 10% (w/w) Folin–Ciocâlteu reagent and left in a dark compartment for 5 min. Subsequently, 1.5 ml of 5% (w/w) Na₂CO₃ solution was added, and the mixture was stored in the dark for 2 h. The absorbance of this mixture was then measured at 750 nm using a spectrophotometer. This analysis was performed for all liquid smoke samples, with three repetitions for each sample.

2.4.3 Antioxidant capacity analysis

The antioxidant capacity was measured following a procedure detailed elsewhere [46]. An ultraviolet-visible (UV-Vis) spectrophotometer was used to monitor chromogen colour changes in DPPH-treated liquid smoke, which occur due to DPPH neutralisation. A 40-ppm DPPH solution was prepared by dissolving 4 mg of DPPH crystals in methanol. This solution was stored in a cold, dark environment to maintain stability. The liquid smoke was dissolved in dimethyl sulphoxide (DMSO) and sonicated for 5 min to ensure the solution was homogeneous. Subsequently, 3 ml of the DPPH solution was mixed with 1.5 ml of the liquid smoke solution. The mixture was gently shaken and then kept in a cold, dark environment for 10 min. The absorbance of the mixture was measured using a UV-Vis spectrophotometer at a wavelength of 518 nm, with three repetitions conducted for each liquid smoke sample. Additionally, 1.5 ml of pure DMSO was used as a

blank sample. The EC50 value was determined by comparing the percentage difference between the absorbance of the mixture and that of the blank sample.

3 Results and discussions

3.1 Thermal properties of EFBs

Both proximate and ultimate analyses on the EFBs result in the following: 16.15% for moisture content, 61.36% for volatile matter content, 17.27% for fixed carbon content, 5.22% for ash content, 52.46% for elemental carbon content, 0.73% for elemental nitrogen content, 6.03% for elemental hydrogen content, and 0.28% for elemental sulphur content. These compositions had almost similar magnitudes to those of both softwood and hardwood, as the traditional raw material of liquid smoke [47]. The main compositional difference was the higher content of ash in EFBs due to the significant presence of silicon and potassium that were accumulated to suppress physical stress and to fulfil nutrient requirements during the oil palm lifetime, respectively [48,49].

3.2 Influence of electroporation on physical properties of EFBs

SEM analysis was performed on EFBs before and after electroporation to examine the impact of the treatment on their microscopic physical structure. The resulting SEM micrographs are presented in Figure 2, offering a visual comparison between untreated and electroporated EFB strands. The left micrograph shows an intact EFB strand, as no electroporation was applied. In contrast, the middle micrograph, corresponding to treatment at

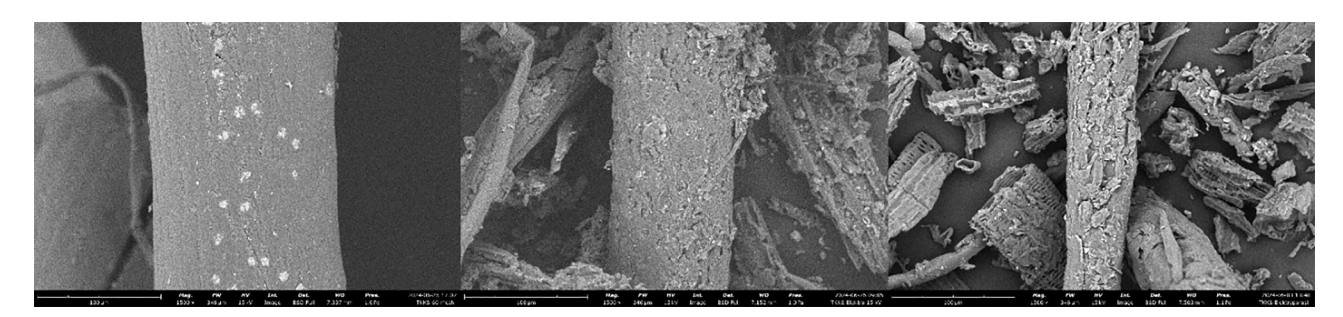


Figure 2: 1,500-Time visual magnification of microstructures of EFB: Left, raw EFBs; middle, EFBs after electroporation at 15 kV·cm⁻¹; right, EFBs after electroporation at 20 kV·cm⁻¹.

15 kV·cm⁻¹, reveals moderate physical damage such as cavities, surface tears, and scratches. The right micrograph depicts more severe structural damage, including deep cavities, breakage, holes, and punctures, following electroporation at 20 kV·cm⁻¹. The progression of damage with increasing electric field strength supports the hypothesis that electroporation enhances the permeability of lignocellulosic material [50]. At 20 kV·cm⁻¹, the electric field was sufficiently intense to rupture the lignocellulosic matrix, leading to the release of cytoplasmic fluid into the surrounding medium and forming numerous pores, consistent with cellular breakdown [51].

To complement the SEM observations, quantitative analyses of the microscopic physical characteristics of EFBs were conducted. These included measurements of pore volume (in cm³ per gram of ground EFB), pore size distributions as functions of both pore volume and surface area, and interpretations of the microscopic mechanisms induced by electroporation, as shown in Figure 3(a)–(d).

Figure 3(a) displays pore volume data in the form of nitrogen adsorption-desorption isotherm curves across different electric field strengths. For untreated EFBs (Ads, 0 kV·cm⁻¹ and Des, 0 kV·cm⁻¹), the curves are nearly flat and approach $0 \text{ cm}^3 \cdot \text{g}^{-1}$, suggesting minimal nitrogen uptake due to the rigid lignocellulosic structure and low intrinsic porosity. The overlap of adsorption and desorption curves indicates the presence of large, well-connected pores. In contrast, at 15 kV·cm⁻¹, the adsorption (Ads, 15 kV·cm⁻¹) and desorption (Des, 15 kV·cm⁻¹) curves exhibit a clear increase in nitrogen uptake with rising relative pressure, signifying a growth in pore volume. This increase likely reflects the formation and deepening of cavities resulting from electroporation-induced cracking of the EFB matrix. The appearance of hysteresis, where the adsorption curve exceeds the desorption curve at higher pressures, further supports the presence of newly formed small-sized pores [52]. At 20 kV·cm⁻¹, the adsorption and desorption curves (Ads and Des, 20 kV·cm⁻¹) follow a similar pattern but with an even higher volume of adsorbed nitrogen, indicating more extensive pore formation under stronger electric fields.

Figure 3(b) shows the pore size distribution as a function of pore volume. For untreated EFBs (Ads and Des, $0 \text{ kV} \cdot \text{cm}^{-1}$), the distribution is dominated by pores larger than 11 nm, with a peak pore volume of approximately $1.6 \text{ cm}^3 \cdot \text{g}^{-1}$. The small difference between the adsorption and desorption curves suggests a well-integrated pore network, consistent with earlier structural observations. After electroporation at $15 \text{ kV} \cdot \text{cm}^{-1}$, the pore size distribution shifts toward smaller pores, peaking at around 15.5 nm, and the adsorption curve reaches nearly $3 \text{ cm}^3 \cdot \text{g}^{-1}$. This

shift indicates the breakdown of larger pores into smaller ones due to structural damage. At 20 kV·cm⁻¹, the pore size distribution remains similar in shape but with a higher maximum pore volume of about 3.5 cm³·g⁻¹, suggesting greater structural alteration [53]. In both treated cases, the adsorption curves exceed the desorption curves, further confirming the presence of fine pores and the resultant hysteresis.

Figure 3(c) presents pore size distribution data relative to surface area. The trend across all conditions (Ads, 0 kV·cm⁻¹, Des, 0 kV·cm⁻¹, Ads, 15 kV·cm⁻¹, Des, 15 kV·cm⁻¹, Ads, 20 kV·cm⁻¹, and Des, 20 kV·cm⁻¹) closely mirrors the patterns observed in Figure 3(b). This consistency reinforces the interpretation that electroporation promotes the formation of small-sized pores, as indicated by the simultaneous increase in both pore volume and surface area at comparable pore size ranges.

3.3 Influence of electroporation on yields and chemical properties of EFBs

Building upon the structural and textural changes, the effects of electroporation on the pyrolytic behaviour of EFBs were further evaluated by examining the liquid smoke yield profiles under MAP. These profiles, presented in Figure 4, illustrate the influence of both pyrolysis temperature (300°C and 400°C) and electric field strength (0, 15, and 20 kV·cm⁻¹) of electroporation on liquid smoke production.

The data show that, irrespective of electroporation, MAP conducted at 400°C generally produced higher liquid smoke yields compared to 300°C. This was attributed to the higher thermal input at 400°C, which facilitated more efficient cleavage of chemical bonds within the EFB matrix and enhanced the condensation of pyrolysis vapours into liquid smoke. At the lower temperature of 300°C, the untreated EFBs yielded the highest amount of liquid smoke, approximately 18%. However, when electroporation at 15 kV·cm⁻¹ was applied as a pretreatment, the yield decreased by around 3%, and further dropped to roughly 7% with 20 kV·cm⁻¹ electroporation. This downward trend suggests that increasing the electric field strength during pretreatment progressively reduces the yield of liquid smoke.

The observed decline in yield was likely a direct consequence of the escalating severity of microscopic structural damage. Electroporation-induced porosity increased the effective surface area and pore volume of EFBs, thereby enhancing internal heat and mass transfer during pyrolysis. For EFBs treated at 15 kV·cm⁻¹, this structural

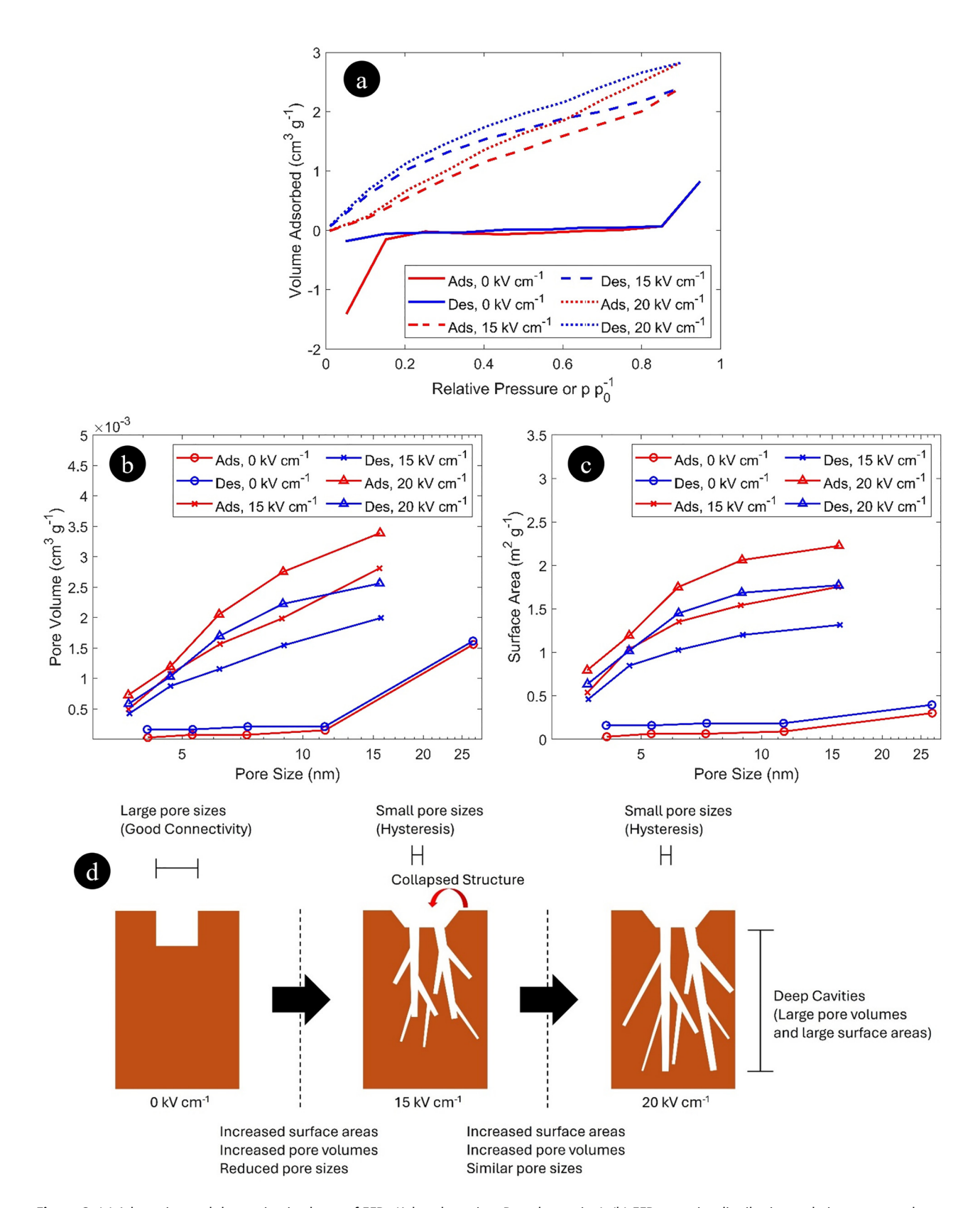


Figure 3: (a) Adsorption and desorption isotherm of EFBs (Ads, adsorption; Des, desorption), (b) EFB pore size distributions relative to pore volumes (Ads, adsorption; Des, desorption), (c) EFB pore size distributions relative to surface areas (Ads, adsorption; Des, desorption), and (d) possible microscopic electroporation mechanism of EFBs.

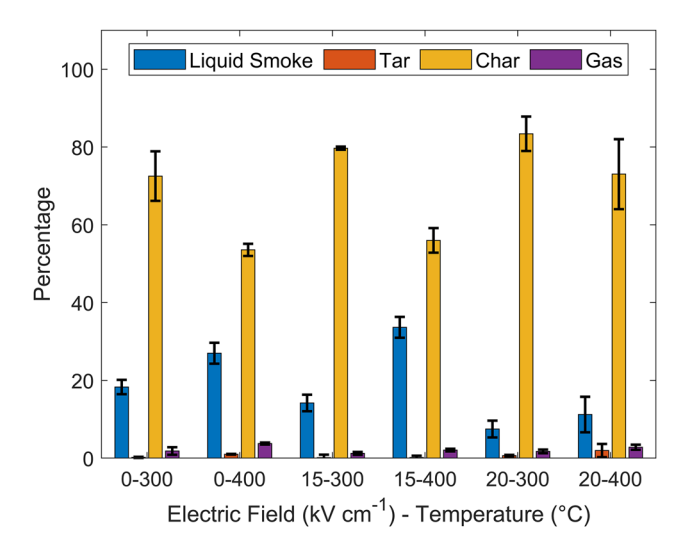


Figure 4: Pyrolytic product yield of EFBs at varying MAP temperatures (p < 0.05) and electric field strength of electroporation (p < 0.05).

modification appeared to facilitate more rapid heating, diminishing product selectivity towards liquid-phase products and shifting the reaction balance toward gas formation. The effect was even more pronounced at 20 kV·cm⁻¹, where the presence of extensive surface cavities and ruptures further accelerated heating and volatile release, resulting in markedly lower liquid smoke yields.

Interestingly, at the elevated pyrolysis temperature of 400°C, the trend differed. Here, electroporation at 15 kV·cm⁻¹ produced a higher liquid smoke yield than the untreated EFBs. This reversal may be explained by the electroporation-induced microstructural disruption, enhancing the accessibility of internal cellulose domains to thermal energy. At 400°C, EFBs undergo significant thermal degradation, which further extends to decomposition of lignin and cellulose than the thermal degradation at 300°C, producing more and heavier phenolic compounds that were more effectively retained and condensed into liquid smoke. In addition, electroporated EFBs at 15 kV·cm⁻¹ via structural damage might have enhanced the volatilisation and the condensation. However, the observed decline in liquid smoke yield at 20 kV·cm⁻¹ suggests that excessively high electric field strengths may induce adverse effects, possibly due to the occurrence of extreme permeabilisation or irreversible electroporation, potentially resulting in significant structural damage or localised cell disintegration. This might have led to premature loss or thermal degradation of key volatile precursors before they were converted into condensable products, ultimately diminishing liquid smoke yield. Additionally, more aggressive electroporation might have increased the susceptibility of intermediate volatiles to further

cracking during pyrolysis, shifting the product distribution away from liquid fractions and towards non-condensable gases and char. Accordingly, while moderate electroporation (e.g. 15 kV·cm⁻¹) appeared beneficial for enhancing yield through improved permeability and volatile release, exceeding this threshold, as with 20 kV·cm⁻¹ resulted in diminishing returns or even detrimental effects on liquid smoke production.

To further understand the chemical transformation of EFBs during pyrolysis, the chemical composition of the resulting liquid smoke was analysed using gas chromatography—mass spectrometry (GC-MS). The results, expressed as normalised mass percentages (relative concentrations) of organic-based compounds, are summarised in Table 1.

At 300°C, the organic fraction of liquid smoke from raw EFB was dominated by phenolic compounds (68.94%), followed by a small fraction of carbonyl-containing compounds (4.15%), and a substantial proportion of unidentified impurities (26.91%) that were neither phenolic, furanic, carbonyl, nor carboxylic in nature. The high proportion of phenolic compounds was unexpected, given that raw EFBs contain over 80% holocellulose [54]. At this temperature, cellulose undergoes depolymerisation into oligosaccharides due to the cleavage of β -(1 \rightarrow 4)-glycosidic bonds [55]. These oligosaccharides subsequently follow three major degradation pathways: (i) dehydration into monomeric sugars such as levoglucosan and levoglucosenone [56,57]; (ii) molecular reconstruction into furanic compounds like furfural and hydroxymethylfurfural [58-60]; and (iii) fragmentation into lighter carbonyl compounds such as acetone and acetol [61,62]. However, only minimal quantities of cellulose-derived compounds were retained in the liquid smoke, possibly due to further degradation into non-condensable gases (e.g., CO and H₂O) during their migration through the heated EFB matrix under microwave irradiation. Some of this degradation may have occurred above the solid bed at slower rates due to weaker microwave penetration in the gas phase [63].

Hemicellulose, which makes up less than 10% of EFBs, begins to degrade at temperatures as low as 200°C due to its amorphous structure. Nonetheless, only trace quantities of hemicellulose-derived compounds were found, such as minor carbonyls, likely originating from the degradation of O-acetyl xylan units [64]. As with cellulose-derived intermediates, many hemicellulose products may have been lost as non-condensable gases before exiting the biomass.

As the temperature approached 300°C, lignin underwent depolymerisation through cleavage of C–O and C=O bonds. While this process typically yields methoxyphenols, the GC-MS results showed phenol as the dominant lignin-derived product, accounting for over 50% of the

organic fraction. This suggests that demethylation and demethoxylation, typically occurring at >350°C, were accelerated by microwave heating even at 300°C [65,66]. The thermal stability of aromatic rings further contributed to the high phenol retention in the liquid smoke [67].

Unexpectedly, diester phthalic acid, a compound of regulatory concern, was present at 12.14%. Its formation may have occurred via a multi-step process: (1) formation of 1-methylnaphthalene from lignin degradation, (2) oxidation into phthalic anhydride, and (3) subsequent esterification with phenol or trace alcohols. Although 1-methylnaphthalene is poorly soluble in water and expected to partition into the heavy phase, co-solubility with phenolic compounds could have facilitated its migration into the water-rich liquid smoke. The rapid heating conditions in MAP may have driven the necessary reactions even at 300°C [68-70].

More than 20% of the organic content consisted of unidentified impurities, as indicated by weak or unresolved GC-MS peaks. These impurities may represent aliphatic compounds formed through ring-opening reactions of C₅ and C₆ sugars or breakdown of furanics [71].

The presence of diester phthalic acid raises critical safety concerns, particularly for food applications. Diester phthalates, such as diethyl and dibutyl phthalates, are recognised endocrine-disrupting and potentially carcinogenic compounds that are strictly regulated by authorities, including the U.S. Food and Drug Administration (FDA) and the European Food Safety Authority (EFSA). To ensure food safety and regulatory compliance, additional purification steps are required before commercialisation. Effective strategies include activated carbon or biochar adsorption to remove hydrophobic contaminants such as phthalates [72]; solid-phase extraction (SPE) for selective isolation; and membrane-based separation methods like nanofiltration or ultrafiltration to remove low-molecularweight compounds [73,74]. These purification techniques should be paired with post-treatment chemical analysis (e.g., GC-MS) to verify the absence or safe levels of phthalates. Preventive measures, such as using phthalate-free equipment and clean biomass feedstock, are also essential to mitigate upstream contamination. A combined approach ensures alignment with food safety standards.

At 400°C, MAP of raw EFBs produced liquid smoke with slightly lower phenolic content (-8.35%) and increased carbonyls (7.68%) compared to that at 300°C. Although the total phenolic proportion declined, several methoxyphenol, including 2-methoxyphenol, 4-ethyl-2methoxyphenol, and 2,6-dimethoxyphenol, appeared in higher concentrations, as temperatures below ~500°C promote methoxyphenol formation before demethoxylation

becomes dominant at higher temperatures [75–77]. The increased carbonyl content at 400°C likely reflects secondary degradation of monomeric sugars into furanics and carbonyls [78]. However, the limited furanic content suggests further degradation of furanics into carbonyls or non-condensable gases due to the instability of oxygenated five-membered rings at this temperature [79]. Additionally, hemicellulose may have contributed more carbonyls via intensified decomposition.

Most carbonyl compounds identified at 400°C were cyclopentene derivatives, possibly formed through ring cracking of furanics or via alkali-catalysed Michael-Aldol condensation and cyclisation [80-82]. The lower yield of lignin-derived compounds at this temperature may be attributed to their reduced thermal stability. Moderate selectivity toward cresol and catechol was observed, potentially arising from methyl radical reactions with methoxyphenol and hydrogen radical interaction with phenoxy radicals, respectively [83]. A rise in unidentified impurities was also recorded at 400°C, indicating increased selectivity for aliphatic compounds at higher pyrolysis temperatures.

Electroporation treatment prior to MAP significantly influenced the chemical composition of the liquid smoke. At 300°C, EFB electroporated at 15 kV·cm⁻¹ produced 7.38% fewer phenolic compounds than untreated EFBs, likely due to partial lignin loss into the electroporation medium. Despite this, phenol, the dominant phenolic compound, increased from 40.69% to 44.41%, suggesting that surface damage enhanced methoxyphenol demethoxylation [84]. In contrast, EFB pre-treated at 20 kV·cm⁻¹ showed a more than 20% reduction in phenolic content compared to untreated EFBs, and lower phenol levels than the 15 kV·cm⁻¹ case, likely due to excessive lignin loss. Both electroporated samples showed low carbonyl selectivity, though 3-furaldehyde appeared at a moderate level (4.7%) in the 20 kV·cm⁻¹ case, likely originating from accelerated cellulose and hemicellulose conversion [85,86]. A similar trend of decreasing phenolic and carbonyl content was observed at 400°C across increasing electric field strengths, likely driven by analogous degradation mechanisms.

To further elucidate the bioactive characteristics of the liquid smoke, total phenolic content (TPC), antioxidant capacity, and acidity were evaluated, as shown in Figure 5(a)-(c). These properties are essential indicators of the functional potential of liquid smoke for food applications, particularly in terms of preservative and antioxidant performance.

Figure 5(a) presents the TPC of the liquid smoke, expressed in milligrams of gallic acid equivalents (GAE) per litre. At 300°C, the TPC decreased progressively from approximately 43 mg GAE/L in raw EFB to 15 mg GAE/L and 13 mg GAE/L following electroporation pretreatment at 15

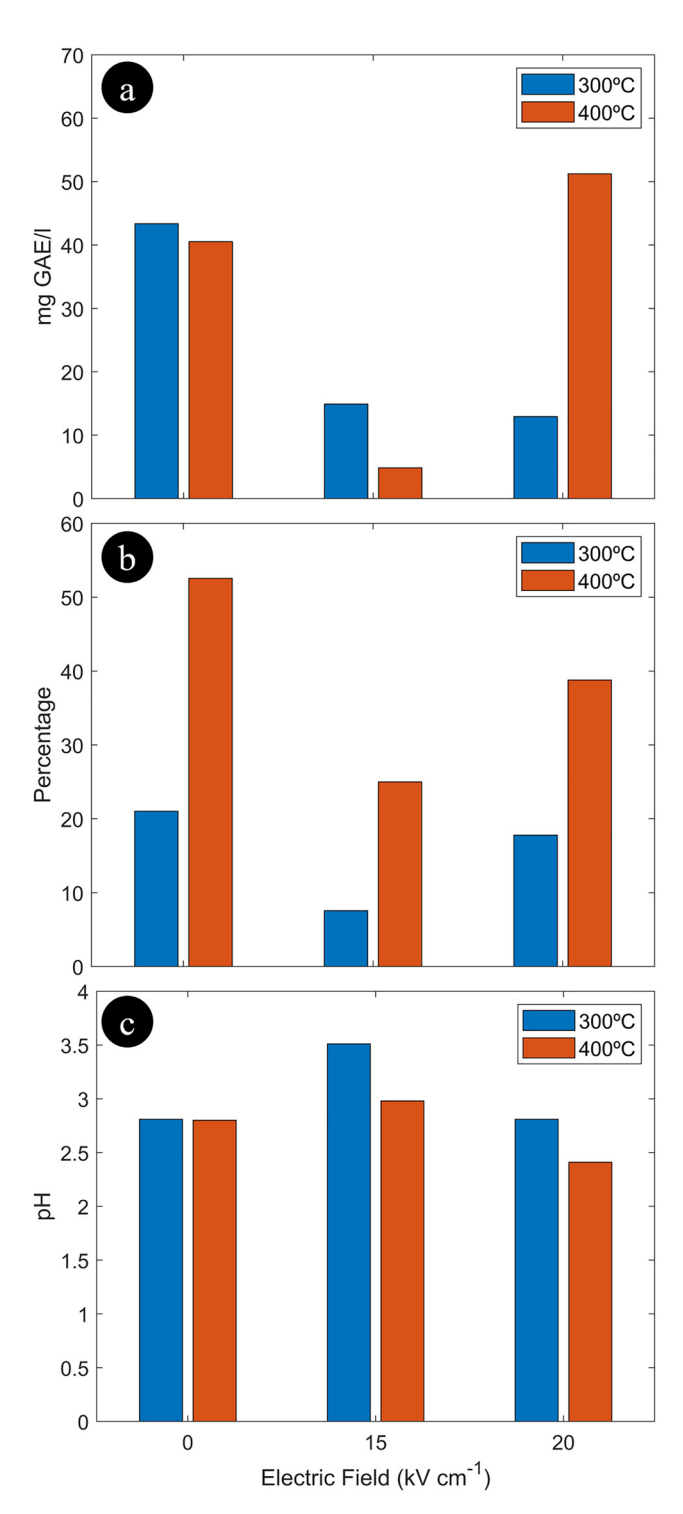


Figure 5: (a) Total phenolic content in liquid smoke (p > 0.05), (b) antioxidant capacity of liquid smoke (p > 0.05), and (c) pH of liquid smoke (p > 0.05).

and 20 kV·cm⁻¹, respectively. This trend corresponds to the decline in phenolic compound mass percentages reported in Table 1. The reduction is likely attributed to the electroporation-induced surface damage, which facilitated the

premature release of volatile phenolic compounds before efficient condensation could occur. At 400°C, however, a different trend was observed. While the TPC initially declined to 4 mg GAE/l after pretreatment at 15 kV·cm⁻¹, it subsequently increased to approximately 52 mg GAE/l at 20 kV·cm⁻¹. This increase may be explained by enhanced lignin depolymerisation and deeper structural breakdown under the synergistic effects of high pyrolysis temperature and stronger electric field, which promoted the formation and retention of additional phenolic compounds in the liquid smoke.

As shown in Figure 5(b), the antioxidant capacity of the liquid smoke exhibited a consistent trend of enhancement at 400°C relative to 300°C, regardless of electroporation intensity. This is likely due to the formation of highly active phenolic compounds such as catechol, 3-methoxy-1,2-benzenediol, and syringylacetone, which were identified in the GC-MS results of the 400°C samples (Table 1) but were either absent or present in negligible amounts at 300°C [87-89]. Notably, at 400°C, antioxidant capacity increased with the electric field strength, reaching 38.8% at 20 kV·cm⁻¹. This increase was accompanied by a drop in pH to 2.41 (Figure 5(c)), reflecting a greater abundance of acidic phenolic compounds. Conversely, at 300°C, higher electric field strengths were associated with reduced antioxidant capacity and elevated pH, suggesting a lower concentration of retained phenolics and acidic compounds. Nevertheless, the pH values of all liquid smoke samples remained within the acceptable range defined by the Japan Liquid Smoke Association, underscoring their potential safety and applicability for food-related use.

Although GC-MS analysis showed a lower proportion total phenolics under certain conditions, the Folin-Ciocalteu method revealed higher TPC values in these same samples, particularly those subjected to 400°C MAP and 20 kV·cm⁻¹ electroporation. This discrepancy may be attributed to the generation of phenolic compounds that are more effectively retained or condensed at high temperatures. Additionally, the presence of other bioactive compounds, such as 3-furaldehyde and cyclopentene, identified in samples produced at higher electric fields and temperatures may have contributed to the overall antioxidant capacity through secondary mechanisms. Though less potent than phenolics, these compounds can act as electron acceptors or radical scavengers via electrophilic addition or conjugated ring stabilisation, thereby enhancing antioxidant properties in a cumulative manner.

Despite these observable trends, statistical analysis indicated that neither electric field strength nor MAP temperature had a statistically significant effect on TPC, antioxidant capacity, or pH (p > 0.05). These results suggest that

the variability in these parameters may be driven by complex synergistic interactions among various chemical constituents in the liquid smoke rather than by the main process variables alone. The co-presence of phenolics and non-phenolic organic compounds, such as furans, carbonyls, and minor aliphatic compounds, may collectively influence antioxidant functionality and acidity through interdependent mechanisms, including hydrogen bonding, redox cycling, and structural rearrangements during pyrolysis.

3.4 Statistical prediction of possible mechanisms of EFB conversion into liquid smoke

To better interpret the complex interrelationship between treatment parameters and the resulting chemical composition of liquid smoke, principal component analysis (PCA) was performed on the GC-MS dataset. This multivariate statistical approach enabled dimensionality reduction, transforming the normalised mass percentages of individual compounds into a set of orthogonal principal components (PCs) that capture the major variance across all samples. The input variables comprised the chemical compounds identified by GC-MS, while the samples were defined by combinations of MAP temperature and electroporation electric field strength. As a result, the number of chemical variables was reduced to five principal components, with the first two, PC1 and PC2, accounting for 81.63% and 10.44% of the total variance, respectively.

The PCA results are summarised in Figure 6(a) and (b), which depict the score and loading plots based on PC1 and PC2. The score plot (Figure 6a) reveals the relative positioning of each sample, where the Euclidean distances reflect differences in chemical compound distributions. The loading plot (Figure 6b), on the other hand, visualises the influence of individual compounds on the observed variance. Chemical species located far from the origin are considered major contributors to either PC1 or PC2, or both.

As shown in Figure 6(a), the samples are broadly scattered along the PC1 axis, indicating that electroporation intensity and MAP temperature induced distinct chemical transformations in the liquid smoke. Notably, the samples generated from EFB pre-treated at 15 kV·cm⁻¹ and pyrolysed at 400°C, and from EFB pre-treated at 20 kV·cm⁻¹ and pyrolysed at 300°C, are positioned closer to each other relative to other sample combinations. This proximity implies that their liquid smokes shared similar chemical profiles, consistent with the GC-MS data in Table 1, and

supports the notion that high-field electroporation can simulate higher-temperature pyrolysis effects through enhanced cell disintegration and lignocellulose accessibility.

The loading plot (Figure 6b) shows that most compounds cluster near the origin, suggesting modest variance contributions. However, a few key compounds, including P1 (phenol), P6 (2,6-dimethoxyphenol), P12 (3-methoxy-1,2benzenediol), P17 (diester phthalic acid), CC2 (2-hydroxy-3methyl-2-cyclopenten-1-one), and I (impurities), reside at significant distances from the origin, indicating a strong influence on the overall variance. A pronounced negative correlation between PC1 and several phenolic compounds is evident, particularly for P1, P6, and P12, located in the western quadrant. As the severity of electroporation increased, a shift toward the eastern quadrant in Figure 6(a) was observed, corresponding to a reduction in phenolic compound abundance. Conversely, the strong positive correlation between PC1 and impurities (I) suggests that elevated electroporation intensities may have promoted the formation of aliphatic degradation products, possibly via ring-opening of sugar- and furan-derived compounds. This finding corroborates prior observations of increased impurity levels in highly electroporated samples

To provide a clearer view of compound separation, a magnified loading plot is presented in Figure 6(c), which facilitates a quadrant-based interpretation of compound grouping and underlying pyrolytic pathways. Compounds were distributed across four quadrants: the southwest (SW), where primary lignin-derived phenolics such as 2-methylphenol and 2,6-dimethylphenol, and several cyclopentene reside - indicating negative correlation with both PCs; the southeast (SE), which includes potent antioxidant phenolics such as catechol, syringylacetone, and 2-methoxy-4-vinylphenol; the northeast (NE), populated by furanic compounds such as 3-furaldehyde and 3-methylfuran; and the northwest (NW), where few compounds were identified. These spatial arrangements imply distinct formation and transformation mechanisms depending on the thermochemical and electroporation conditions.

Based on the compound distribution patterns observed in Figure 6(b) and (c), a proposed degradation pathway is illustrated in Figure 7. The pathway integrates known thermochemical conversion mechanisms of lignocellulosic biomass, specifically targeting the degradation of cellulose, hemicellulose, and lignin in EFBs [71,90-93]. As MAP temperatures increased toward 300°C, cellulose and hemicellulose underwent dehydration and glycosidic bond cleavage, yielding C5 and C6 sugar derivatives such as xylose and levoglucosan. These intermediates subsequently transformed into furanic compounds (e.g.,

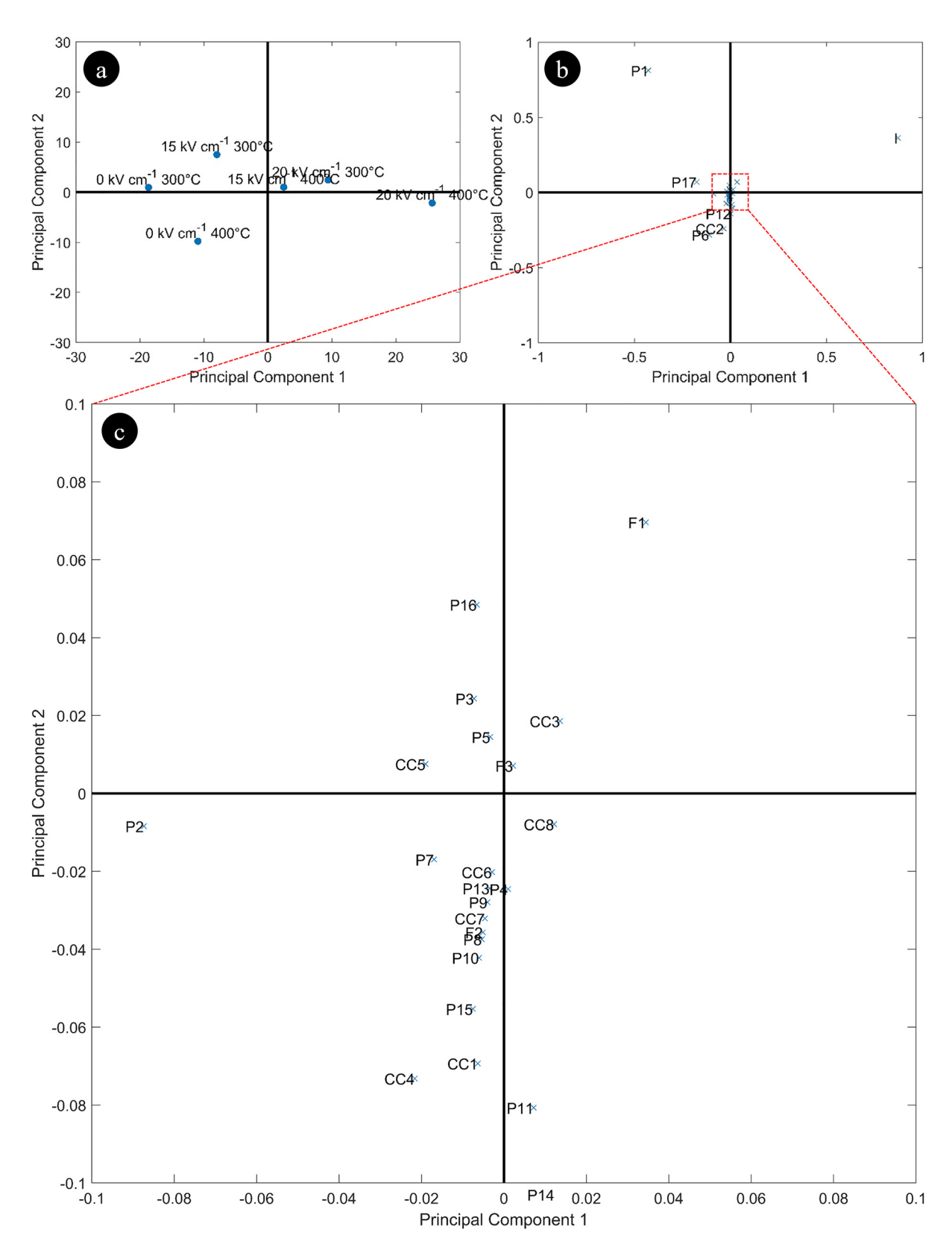
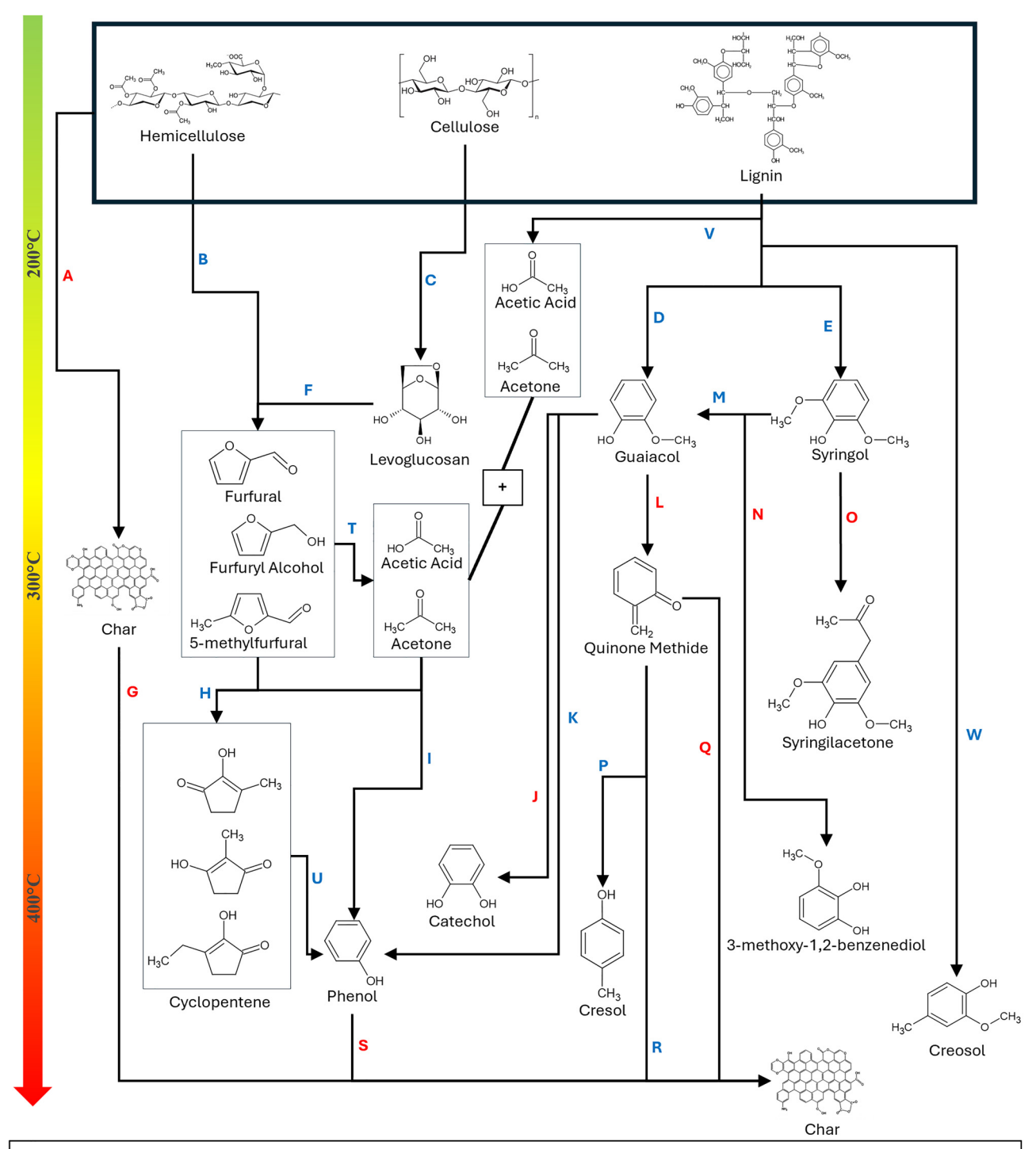


Figure 6: (a) Score plot of PC1 and PC2 for GC-MS analysis results: 0 kV·cm⁻¹ 300°C, MAP of raw EFB at 300°C; 15 kV·cm⁻¹ 300°C, MAP at 300°C of EFB electroporated at 15 kV·cm⁻¹; 20 kV·cm⁻¹ 300°C, MAP at 300°C of EFB electroporated at 20 kV·cm⁻¹; 0 kV·cm⁻¹ 400°C, MAP of raw EFB at 400°C; 15 kV·cm⁻¹ 400°C, MAP at 400°C of EFB electroporated at 15 kV·cm⁻¹; 20 kV·cm⁻¹ 400°C, MAP at 400°C of EFB electroporated at 20 kV·cm⁻¹, (b, c) loading plot of PC1 and P2 for GC-MS analysis results: chemical compound IDs are listed in Table 1.



A: polymerization; B: depolymerization and ring opening; C: depolymerization; D: decomposition; E: decomposition; F: ring-opening; G: polymerization; H: aldol condensation, cyclization, and dehydration; I: aromatization; J,K: demethylation; L: dehydrogenation; M: demethoxylation; N: demethylation; O: demethylation; P: proton addition; Q: polymerization; R: polymerisation; S: polymerization; T: ring-opening; U: aromatization; V: debranching; W: decomposition; RED: in which the product is favored due to high electric field electroporation; BLUE: in which the product is favored due to low electric field electroporation

Figure 7: The possible mechanism of thermal degradation of electroporated EFBs during MAP.

furfural), which, under continued heating, degraded into smaller carbonyl compounds and cyclopentene. Although cyclopentene was detected in small quantities, its formation appeared thermodynamically favourable under moderate heating conditions, particularly for mildly electroporated EFBs.

The lignin degradation pathway was temperature- and structure-dependent, primarily influenced by the guaiacyl (G) and syringyl (S) subunits in EFB lignin, which has a G/S ratio of 0.411 ± 0.003 [94]. At 200–300°C, cleavage of ether bonds yielded 2-methoxyphenol (guaiacol) and 2,6-dimethoxyphenol (syringol). Interestingly, the concentrations of these methoxylated phenolics declined with increasing electroporation field strength, likely due to rapid heating and increased exposure that accelerated secondary degradation. Furthermore, the near-equal abundance of guaiacol and syringol, despite the expected dominance of syringol, suggests a partial conversion of syringyl-type compounds into guaiacyl-type compounds during MAP.

Between 300°C and 400°C, additional demethoxylation, demethylation, and structural rearrangements of guaiacol occurred. These reactions favoured the formation of phenol, catechol, and cresol. Samples subjected to higher electric fields exhibited increased concentrations of catechol and cresol, compounds associated with potent antioxidant activity (see Figure 5b). These may have originated from radical pathways involving guaiacol transformation into quinone methide, followed by methide hydrogenation and methoxylation reactions. Meanwhile, 2,6-dimethoxyphenol could be transformed into 3-methoxy-1,2-benzenediol and syringylacetone via demethoxylation and ketone chain insertion, processes that were moderately favoured under severe electroporation, as evidenced by the enhanced antioxidant performance.

In summary, the PCA results, combined with compound-specific analyses and mechanistic interpretation, suggest that both MAP temperature and electroporation intensity influence not only the quantity but also the quality and reactivity of compounds formed in liquid smoke. However, given that the p-values for the effects of electroporation and MAP temperature on total phenolic content, antioxidant capacity, and pH were statistically insignificant (p > 0.05), it is likely that synergistic interactions among multiple compound classes – particularly between phenolic and non-phenolic organics - govern the observed chemical and functional outcomes. Such interdependencies underscore the complex nature of pyrolytic transformations and highlight the importance of integrated chemical, statistical, and mechanistic approaches for optimising bioactive compound production.

4 Conclusions

Electroporation was applied to EFBs prior to MAP to investigate the combined effects of these treatments on the characteristics of the resulting liquid smoke. This study provides a more comprehensive understanding of how electroporation and MAP influence liquid smoke properties compared to the initial hypothesis. The hypothesis suggested that applying a high electric field to EFBs would potentially reduce the liquid smoke yield, increase its antioxidant capacity, and lower its acidity, while the MAP of electroporated EFBs would negatively affect the antioxidant capacity due to secondary cracking of phenolic compounds at low temperatures. The results revealed that electroporation significantly altered the physical properties of EFBs, with higher electric fields causing greater structural disruptions. These structural changes influenced the characteristics of the liquid smoke produced through MAP. The disruptions were evident from reduced EFB pore sizes as the electric field intensity increased during electroporation. Notably, the MAP of EFBs treated with an electric field of 15 kV·cm⁻¹ produced a relatively high liquid smoke vield, whereas EFBs subjected to an electric field of 20 kV·cm⁻¹ resulted in a lower yield. Interestingly, the liquid smoke derived from MAP of EFBs electroporated at 20 kV·cm⁻¹ exhibited higher antioxidant capacity and lower pH compared to that from EFBs electroporated at 15 kV·cm⁻¹. This outcome may suggest that structural disruption induced by the electric field at elevated temperatures facilitates more extensive lignocellulosic decomposition, leading to the formation of phenolic compounds that are more readily extractable and condensible into the liquid phase. The enhanced antioxidant capacity and reduced pH were attributed to the combined effects of MAP and, more critically, the high electric field during electroporation, which improved the selectivity of chemical compounds with high antioxidant properties and acidity. Additionally, some compounds displayed selectivity when lower electric fields were applied during electroporation. Based on the chemical compounds identified in the liquid smoke, the study proposed a thermal degradation mechanism for lignocellulose. This mechanism included detailed guidelines on how MAP temperatures and electroporation electric fields contributed to specific chemical conversion pathways. Overall, this study offers valuable insights into the valorisation of EFBs, an abundant agricultural waste material. Future research should focus on optimising electroporation and MAP operating conditions to improve the yield and functionality of the liquid smoke produced.

Acknowledgments: This work was supported by the Directorate of Research and Community Service at

Institut Teknologi Sepuluh Nopember via the scheme of Dana Keilmuan ITS (1171/PKS/ITS/2024) and the National Research and Innovation Agency and the Endowment Fund for Education Agency via the scheme of Riset dan Inovasi untuk Indonesia Maju (3871/II.7.5/KS.00/4/2025 and 2599/III.10/FR.06.00/4/2025).

Funding information: The authors state that this work was funded by the Directorate of Research and Community Service at Institut Teknologi Sepuluh Nopember via the scheme of Dana Keilmuan ITS (1171/PKS/ITS/2024) and the National Research and Innovation Agency and the Endowment Fund for Education Agency via the scheme of Riset dan Inovasi untuk Indonesia Maju (3871/II.7.5/ KS.00/4/2025 and 2599/III.10/FR.06.00/4/2025).

Author contributions: Wahyu Meka: conceptualisation, methodology, writing - original draft, visualisation, supervision, project administration, funding acquisition. Orchidea Rachmaniah: validation, formal analysis, resources, writing – review & editing, supervision. Rijalul Mulhim Al-Mauhub: investigation, data curation. Nathanael Abishai Widiraga: investigation, data curation. Ratri Safira Tirta Afida: investigation, data curation. Patricia Evangeline Toqueville Purba: investigation, data curation. Latifa Hanum Lalasari: investigation, resources. Anugerah Dany Priyanto: investigation, resources. Henni Vanda: investigation, resources. Mahardika Fahrudin Rois: investigation, resources, writing - review & editing. Yulia Fitri: writing – review & editing. Salman Masoudi Soltani: writing - review & editing.

Conflict of interest: The authors state no conflict of interest.

Data availability statement: All data generated or analysed during this study are included in this published article (and its supplementary information files).

References

- Hasan MM, Al Amin M, Arefin MS, Mostafa T. Green consumers' behavioral intention and loyalty to use mobile organic food delivery applications: The role of social supports, sustainability perceptions, and religious consciousness. Env Dev Sustain. 2024;26(6):15953-6003. doi: 10.1007/s10668-023-03284-z.
- Basha MB, Mason C, Shamsudin MF, Hussain HI, Salem MA. Consumers attitude towards organic food. Procedia Econ Financ. 2015;31:444-52. doi: 10.1016/S2212-5671(15)01219-8.
- Maleki F, Yaghoubi S, Fander A. Organic level vs. sales effort in coordination of green food supply chain for deteriorating items.

- Env Dev Sustain. 2023;25(11):13065-97. doi: 10.1007/s11625-022-
- [4] Lingbeck JM, Cordero P, O'Bryan CA, Johnson MG, Ricke SC, Crandall PG. Functionality of liquid smoke as an all-natural antimicrobial in food preservation. Meat Sci. 2014;97(2):197-206. doi: 10.1016/j.meatsci.2014.02.003.
- Yang E, Jun M, Haijun H, Wenfu C. Chemical composition and potential bioactivity of volatile from fast pyrolysis of rice husk. J Anal Appl Pyrolysis. 2015;112:394-400. doi: 10.1016/j.jaap.2015.02.021.
- Research and Markets. Liquid smoke market report: Trends, [6] forecast and competitive analysis to 2030. Dallas, TX, USA: Lucintel; 2024. https://www.researchandmarkets.com/reports/5993476/ liquid-smoke-market-report-trends-forecast.
- [7] Pimenta AS, da Costa Monteiro TV, Fasciotti M, Braga RM, de Souza EC, de Lima KMG. Fast pyrolysis of trunk wood and stump wood from a Brazilian eucalyptus clone. Ind Crop Prod. 2018;125:630-8. doi: 10.1016/j.indcrop.2018.08.083.
- Xin X, Dell K, Udugama IA, Young BR, Baroutian S. Transforming biomass pyrolysis technologies to produce liquid smoke food flavouring. J Clean Prod. 2021;294:125368. doi: 10.1016/j.jclepro. 2020.125368.
- Hua F, Bruijnzeel LA, Meli P, Martin PA, Zhang J, Nakagawa S, et al. [9] The biodiversity and ecosystem service contributions and tradeoffs of forest restoration approaches. Science. 2022;376(6595):839-44. doi: 10.1126/science.abl4649.
- Panja P. Deforestation, carbon dioxide increase in the atmosphere and global warming: A modelling study. Int | Model Simul. 2021;41(3):209-19. doi: 10.1080/02286203.2019.1707501.
- Noirot LM, Müller-Stöver DS, Wahyuningsih R, Sørensen H, [11] Simamora A, Caliman JP. Impacts of empty fruit bunch applications on soil organic carbon in an industrial oil palm plantation. J Env Manage. 2022;317:115373. doi: 10.1016/j.jenvman.2022.115373.
- Chin SX, Chia CH, Zakaria S, Fang Z, Ahmad S. Ball milling pretreatment and diluted acid hydrolysis of oil palm empty fruit bunch (EFB) fibres for the production of levulinic acid. J Taiwan Inst Chem Eng. 2015;52:85-92. doi: 10.1016/j.jtice.2015.01.028.
- Krishnan Y, Bong CPC, Azman NF, Zakaria Z, Abdullah N, Ho CS, et al. Co-composting of palm empty fruit bunch and palm oil mill effluent: Microbial diversity and potential mitigation of greenhouse gas emission. J Clean Prod. 2017;146:94-100. doi: 10.1016/j.jclepro. 2016.08.118.
- [14] Bouza RJ, Gu Z, Evans JH. Screening conditions for acid pretreatment and enzymatic hydrolysis of empty fruit bunches. Ind Crop Prod. 2016;84:67-71. doi: 10.1016/j.indcrop.2016.01.041.
- [15] Abdullah N, Gerhauser H. Bio-oil derived from empty fruit bunches. Fuel. 2008;87(12):2606-13. doi: 10.1016/j.fuel.2008.02.011.
- Sukiran MA, Chin CM, Bakar NK. Bio-oils from pyrolysis of oil palm empty fruit bunches. Am J Appl Sci. 2009;6(5):869-75. doi: 10.3844/ ajas.2009.869.875.
- Abdullah N, Gerhauser H, Sulaiman F. Fast pyrolysis of empty fruit bunches. Fuel. 2010;89(8):2166-9. doi: 10.1016/j.fuel.2009.12.019.
- Sulaiman F, Abdullah N. Optimum conditions for maximising pyrolysis liquids of oil palm empty fruit bunches. Energy. 2011;36(5):2352-9. doi: 10.1016/j.energy.2010.12.067.
- [19] Auta M, Ern LM, Hameed BH. Fixed-bed catalytic and non-catalytic empty fruit bunch biomass pyrolysis. J Anal Appl Pyrolysis. 2014;107:67-72. doi: 10.1016/j.jaap.2014.02.004.
- [20] Alias NB, Ibrahim N, Hamid MKA. Pyrolysis of empty fruit bunch by thermogravimetric analysis. Energy Procedia. 2014;61:2532-6. doi: 10.1016/j.egypro.2014.12.039.

- [21] Sembiring KC, Rinaldi N, Simanungkalit SP. Bio-oil from fast pyrolysis of empty fruit bunch at various temperature. Energy Procedia. 2015;65:162–9. doi: 10.1016/j.egypro.2015.01.052.
- [22] Shafaghat H, Lee HW, Tsang YF, Oh D, Jae J, Jung SC, et al. In-situ and ex-situ catalytic pyrolysis/co-pyrolysis of empty fruit bunches using mesostructured aluminosilicate catalysts. Chem Eng J. 2019;366:330–8. doi: 10.1016/j.cej.2019.02.055.
- [23] Ferreira MFP, Oliveira BFH, Pinheiro WBS, Correa NF, França LF, Ribeiro NFP. Generation of biofuels by slow pyrolysis of palm empty fruit bunches: Optimization of process variables and characterization of physical-chemical products. Biomass Bioenergy. 2020;140:105707. doi: 10.1016/j.biombioe.2020.105707.
- [24] Faisal M, Gani A, Mulana F, Desvita H, Kamaruzzaman S. Effects of pyrolysis temperature on the composition of liquid smoke derived from oil palm empty fruit bunches. Rasayan J Chem. 2020;13(1):514–20. doi: 10.31788/RJC.2020.1315507.
- [25] Sukumar V, Manieniyan V, Senthilkumar R, Sivaprakasam S. Production of bio oil from sweet lime empty fruit bunch by pyrolysis. Renew Energy. 2020;146:309–15. doi: 10.1016/j.renene. 2019.06.156.
- [26] Halim SA, Mohd NA, Razali NA. A comparative assessment of biofuel products from rice husk and oil palm empty fruit bunch obtained from conventional and microwave pyrolysis. J Taiwan Inst Chem Eng. 2022;134:104305. doi: 10.1016/j.jtice.2022.104305.
- [27] Garcia-Nunez JA, Pelaez-Samaniego MR, Garcia-Perez ME, Fonts I, Abrego J, Westerhof RJM, et al. Historical developments of pyrolysis reactors: A review. Energy Fuels. 2017;31(6):5751–75. doi: 10.1021/ acs.energyfuels.7b00641.
- [28] Cao JP, Xiao XB, Zhang SY, Zhao XY, Sato K, Ogawa Y, et al. Preparation and characterization of bio-oils from internally circulating fluidized-bed pyrolyses of municipal, livestock, and wood waste. Bioresour Technol. 2011;102(2):2009–15. doi: 10.1016/j. biortech.2010.09.057.
- [29] Eaton AM, Smoot LD, Hill SC, Eatough CN. Components, formulations, solutions, evaluation, and application of comprehensive combustion models. Prog Energy Combust Sci. 1999;25(4):387–436. doi: 10.1016/S0360-1285(99)00008-8.
- [30] Haque KE. Microwave energy for mineral treatment processes—a brief review. Int J Min Process. 1999;57(1):1–24. doi: 10.1016/S0301-7516(99)00009-5.
- [31] Bengtsson N. Development of industrial microwave heating of foods in Europe over the past 30 years. J Microw Power Electromagn Energy. 2001;36(4):227–40. doi: 10.1080/08327823. 2001.11688464.
- [32] Golberg A, Sack M, Teissie J, Pataro G, Pliquett U, Saulis G, et al. Energy-efficient biomass processing with pulsed electric fields for bioeconomy and sustainable development. Biotechnol Biofuels. 2016;9:1–22. doi: 10.1186/s13068-016-0508-z.
- [33] Maza MA, Martínez JM, Delso C, Camargo A, Raso J, Álvarez I. PEF-dependency on polyphenol extraction during maceration/ fermentation of Grenache grapes. Innov Food Sci Emerg Technol. 2020;60:102303. doi: 10.1016/j.ifset.2020.102303.
- [34] Kumar P, Barrett DM, Delwiche MJ, Stroeve P. Pulsed electric field pretreatment of switchgrass and wood chip species for biofuel production. Ind Eng Chem Res. 2011;50(19):10996–1001. doi: 10. 1021/ie200555u.
- [35] Szwarc D, Szwarc K. Use of a pulsed electric field to improve the biogas potential of maize silage. Energies. 2020;14(1):119. doi: 10. 3390/en14010119.

- [36] Szwarc D, Głowacka K. Increasing the biogas potential of rapeseed straw using pulsed electric field pre-treatment. Energies. 2021;14(24):8307. doi: 10.3390/en14248307.
- [37] Robin A, Sack M, Israel A, Frey W, Müller G, Golberg A. Deashing macroalgae biomass by pulsed electric field treatment. Bioresour Technol. 2018;255:131–9. doi: 10.1016/j.biortech.2018.01.089.
- [38] Kiełbasa P, Dróżdż T, Popardowski E. Influence of coniferous wood conditioning by pulsed electric field on its combustion heat characteristics. Appl Sci. 2021;11(3):983. doi: 10.3390/app11030983.
- [39] Popardowski E, Kiełbasa P. Influence of broadleaved wood conditioning by pulsed electric field on its combustion heat characteristics. Appl Sci. 2022;12(10):5048. doi: 10.3390/app12105048.
- [40] Xin X, Bissett A, Wang J, Gan A, Dell K, Baroutian S. Production of liquid smoke using fluidised-bed fast pyrolysis and its application to green lipped mussel meat. Food Control. 2021;124:107874. doi: 10.1016/j.foodcont.2021.107874.
- [41] Bridgwater AV. Review of fast pyrolysis of biomass and product upgrading. Biomass Bioenergy. 2012;38:68–94. doi: 10.1016/j. biombioe.2011.01.048.
- [42] Montazeri N, Oliveira AC, Himelbloom BH, Leigh MB, Crapo CA. Chemical characterization of commercial liquid smoke products. Food Sci Nutr. 2013;1(1):102–15. doi: 10.1002/fsn3.9.
- [43] Noonan MJ, Tinnesand HV, Buesching CD. Normalizing gaschromatography–mass spectrometry data: method choice can alter biological inference. BioEssays. 2018;40(6):1700210. doi: 10. 1002/bies.201700210.
- [44] Snyder LR, Kirkland JJ, Dolan JW. Introduction to modern liquid chromatography. 3rd edn. Hoboken, NJ, USA: John Wiley & Sons; 2002.
- [45] Xin X, Zhao W, Essien S, Dell K, Baroutian S. The effects of ageing treatment on bioactive contents and chemical composition of liquid smoke food flavourings. Eur Food Res Technol. 2022;248(5):1311–9. doi: 10.1007/s00217-022-03976-2.
- [46] Xiao F, Xu T, Lu B, Liu R. Guidelines for antioxidant assays for food components. Food Front. 2020;1(1):60–9. doi: 10.1002/fft2.10.
- [47] Kim YM, Han TU, Hwang B, Lee B, Lee HW, Park YK, et al. Pyrolysis kinetics and product properties of softwoods, hardwoods, and the nut shell of softwood. Korean J Chem Eng. 2016;33:2350–8. doi: 10. 1007/s11814-016-0142-2.
- [48] Santi LP, Kalbuadi DN, Goenadi DH. Empty fruit bunches as potential source for biosilica fertilizer for oil palm. J Trop Biodivers Biotechnol. 2019;4(3):90–6. doi: 10.22146/jtbb.38749.
- [49] Manning DA. Mineral sources of potassium for plant nutrition. A review. Agron Sustain Dev. 2010;30:281–94. doi: 10.1051/agro/ 2009023
- [50] Kotnik T, Frey W, Sack M, Meglič SH, Peterka M, Miklavčič D. Electroporation-based applications in biotechnology. Trends Biotechnol. 2015;33(8):480–8. doi: 10.1016/j.tibtech.2015.06.002.
- [51] Capodaglio AG. Pulse electric field technology for wastewater and biomass residues' improved valorization. Processes. 2021;9(5):736. doi: 10.3390/pr9050736.
- [52] Fan R, Wang L, Fan J, Sun W, Dong H. The pulsed electric field assisted-extraction enhanced the yield and the physicochemical properties of soluble dietary fiber from orange peel. Front Nutr. 2022;9:925642. doi: 10.3389/fnut.2022.925642.
- [53] Kovačić Đ, Rupčić S, Kralik D, Jovičić D, Spajić R, Tišma M. Pulsed electric field: An emerging pretreatment technology in a biogas production. Waste Manag. 2021;120:467–83. doi: 10.1016/j.wasman. 2020.10.009.

- [54] Konsomboon S, Pipatmanomai S, Madhiyanon T, Tia S. Effect of kaolin addition on ash characteristics of palm empty fruit bunch (EFB) upon combustion. Appl Energy. 2011;88(1):298-305. doi: 10. 1016/j.apenergy.2010.07.008.
- [55] Evans RJ, Milne TA. Molecular characterization of the pyrolysis of biomass. Energy Fuels. 1987;1(2):123-37. doi: 10.1021/ef00002a001.
- [56] Gao Z, Li N, Yin S, Yi W. Pyrolysis behavior of cellulose in a fixed bed reactor: residue evolution and effects of parameters on products distribution and bio-oil composition. Energy. 2019;175:1067-74. doi: 10.1016/j.energy.2019.03.094.
- [57] Assary RS, Curtiss LA. Thermochemistry and reaction barriers for the formation of levoglucosenone from cellobiose. ChemCatChem. 2012;4(2):200-5. doi: 10.1002/cctc.201100280.
- [58] Mayes HB, Nolte MW, Beckham GT, Shanks BH, Broadbelt LI. The alpha-bet (a) of glucose pyrolysis: computational and experimental investigations of 5-hydroxymethylfurfural and levoglucosan formation reveal implications for cellulose pyrolysis. ACS Sustain Chem Eng. 2014;2(6):1461-73. doi: 10.1021/sc500113m.
- [59] Lu Q, Liao HT, Zhang Y, Zhang JJ, Dong CQ. Reaction mechanism of low-temperature fast pyrolysis of fructose to produce 5hydroxymethyl furfural. | Fuel Chem Technol. 2013;41(9):1070-6. doi: 10.1016/S1872-5813(13)60044-4.
- [60] Hu B, Lu Q, Jiang X, Dong X, Cui M, Dong C, et al. Pyrolysis mechanism of glucose and mannose: The formation of 5-hydroxymethyl furfural and furfural. J Energy Chem. 2018;27(2):486-501. doi: 10.1016/j.jechem.2017.11.013.
- [61] Shen DK, Gu S. The mechanism for thermal decomposition of cellulose and its main products. Bioresour Technol. 2009;100(24):6496-504. doi: 10.1016/j.biortech.2009.06.095.
- [62] Zhang Y, Liu C, Xie H. Mechanism studies on β-d-glucopyranose pyrolysis by density functional theory methods. J Anal Appl Pyrolysis. 2014;105:23-34. doi: 10.1016/j.jaap.2013.09.016.
- [63] Polaert I, Estel L, Huyghe R, Thomas M. Adsorbents regeneration under microwave irradiation for dehydration and volatile organic compounds gas treatment. Chem Eng J. 2010;162(3):941-8. doi: 10. 1016/j.cej.2010.06.047.
- [64] Shen DK, Gu S, Bridgwater AV. Study on the pyrolytic behaviour of xylan-based hemicellulose using TG-FTIR and Py-GC-FTIR. J Anal Appl Pyrolysis. 2010;87(2):199-206. doi: 10.1016/j.jaap.2009.12.001.
- [65] Yeo IY, Chin BLF, Tan IK, Loh YS, Comparative studies on the pyrolysis of cellulose, hemicellulose, and lignin based on combined kinetics. J Energy Inst. 2019;92(1):27-37. doi: 10.1016/j.joei.2017.12.003.
- [66] De Bruyn M, Budarin VL, Sturm GS, Stefanidis GD, Radoiu M, Stankiewicz A, et al. Subtle microwave-induced overheating effects in an industrial demethylation reaction and their direct use in the development of an innovative microwave reactor. J Am Chem Soc. 2017;139(15):5431-6. doi: 10.1021/jacs.7b00689.
- [67] Crimmin MR. Benzene rings broken for chemical synthesis. Nature. 2021;597:33-4. doi: 10.1038/d41586-021-02322-y.
- [68] Zhou H, Wu C, Meng A, Zhang Y, Williams PT. Effect of interactions of biomass constituents on polycyclic aromatic hydrocarbons (PAH) formation during fast pyrolysis. J Anal Appl Pyrolysis. 2014;110:264-9. doi: 10.1016/j.jaap.2014.09.007.
- [69] Nuti F, Hildenbrand S, Chelli M, Wodarz R, Papini AM. Synthesis of DEHP metabolites as biomarkers for GC-MS evaluation of phthalates as endocrine disrupters. Bioorg Med Chem. 2005;13(10):3461-5. doi: 10.1016/j.bmc.2005.03.005.
- [70] Rindone B, Saliu F, Suarez-Bertoa R. The synthesis of phthalic anhydride via ozonation of naphthalene. Ozone Sci Eng. 2010;32(3):161-5. doi: 10.1080/01919511003788001.

- [71] Xue P, Liu M, Yang H, Zhang H, Chen Y, Hu Q, et al. Mechanism study on pyrolysis interaction between cellulose, hemicellulose, and lignin based on photoionization time-of-flight mass spectrometer (PI-TOF-MS) analysis. Fuel. 2023;338:127276. doi: 10. 1016/j.fuel.2022.127276.
- Mohan SV, Shailaja S, Krishna MR, Sarma PN. Adsorptive removal of phthalate ester (Di-ethyl phthalate) from aqueous phase by activated carbon: A kinetic study. J Hazard Mater. 2007;146(1-2):278-82. doi: 10.1016/j.jhazmat.2006.12.020.
- [73] Fatoki OS, Noma A. Solid phase extraction method for selective determination of phthalate esters in the aquatic environment. Water Air Soil Pollut. 2002;140:85-98. doi: 10.1023/ A:1020134707450.
- [74] Lim EQ, Seah MQ, Lau WJ, Hasbullah H, Goh PS, Ismail AF, et al. Evaluation of surface properties and separation performance of NF and RO membranes for phthalates removal. Membranes. 2023;13(4):413. doi: 10.3390/membranes13040413.
- [75] Jiang G, Nowakowski DJ, Bridgwater AV. Effect of the temperature on the composition of lignin pyrolysis products. Energy Fuels. 2010;24(8):4470-5. doi: 10.1021/ef100363c.
- [76] Jegers HE, Klein MT. Primary and secondary lignin pyrolysis reaction pathways. Ind Eng Chem Process Des Dev. 1985;24(1):173-83. doi: 10.1021/i200028a030.
- Drage TC, Vane CH, Abbott GD. The closed system pyrolysis of β-O-4 lignin substructure model compounds. Org Geochem. 2022;33(12):1523-31. doi: 10.1016/S0146-6380(02)00119-5.
- Ansari KB, Arora JS, Chew JW, Dauenhauer PJ, Mushrif SH. Fast pyrolysis of cellulose, hemicellulose, and lignin: Effect of operating temperature on bio-oil yield and composition and insights into the intrinsic pyrolysis chemistry. Ind Eng Chem Res. 2019;58(35):15838-52. doi: 10.1021/acs.iecr.9b00920.
- Cureton LT, Napadensky E, Annunziato C, La Scala JJ. The effect of furan molecular units on the glass transition and thermal degradation temperatures of polyamides. J Appl Polym Sci. 2017;134(46):45514. doi: 10.1002/app.45514.
- [80] Wang YZ, Zhang L, Xu T, Ding K. Improving lignocellulose enzymatic saccharification in a bioreactor with an applied electric field. Ind Crop Prod. 2017;109:404-9. doi: 10.1016/j.indcrop.2017.08.061.
- Kröger M, Hartmann F, Klemm M. Hydrothermal treatment of carboxy-methyl cellulose salt: Formation and decomposition of furans, pentenes and benzenes. Chem Eng Technol. 2013;36(2):287-94. doi: 10.1002/ceat.201200468.
- [82] Hong BC, Dange NS, Hsu CS, Liao JH. Sequential organocatalytic stetter and michael-aldol condensation reaction: Asymmetric synthesis of fully substituted cyclopentenes via a [1 + 2 + 2] annulation strategy. Org Lett. 2010;12(21):4812-5. doi: 10.1021/ol101969t.
- Shen DK, Gu S, Luo KH, Wang SR, Fang MX. The pyrolytic [83] degradation of wood-derived lignin from pulping process. Bioresour Technol. 2010;101(15):6136-46. doi: 10.1016/j.biortech. 2010.02.078.
- [84] An Y, Dou J, Tian L, Zhao X, Yu J. Role of microwave during microwave-assisted catalytic reforming of guaiacol, syringolbio-oil as model compounds. J Anal Appl Pyrolysis. 2021;158:105290. doi: 10.1016/j.jaap.2021.105290.
- [85] Hubble AH, Goldfarb JL. Synergistic effects of biomass building blocks on pyrolysis gas and bio-oil formation. J Anal Appl Pyrolysis. 2021;156:105100. doi: 10.1016/j.jaap.2021.105100.
- [86] Patwardhan PR, Brown RC, Shanks BH. Product distribution from the fast pyrolysis of hemicellulose. ChemSusChem. 2011;4(5):636-43. doi: 10.1002/cssc.201000425.

- [87] Kajiyama T, Ohkatsu Y. Effect of para-substituents of phenolic antioxidants. Polym Degrad Stab. 2001;71(3):445–52. doi: 10.1016/ S0141-3910(00)00196-8.
- [88] Ohkatsu Y, Suzuki F. Synergism between phenolic antioxidants in autoxidation. J Jpn Pet Inst. 2011;54(1):22–9. doi: 10.1627/jpi. 54.22.
- [89] Tehan BG, Lloyd EJ, Wong MG, Pitt WR, Montana JG, Manallack DT, et al. Estimation of pKa using semiempirical molecular orbital methods. Part 1: Application to phenols and carboxylic acids. Mol Inf. 2022;21(5):457–72. doi: 10.1002/1521-3838(200211)21:5% 3C457::AID-QSAR457%3E3.0.CO;2-5.
- [90] Chen D, Cen K, Zhuang X, Gan Z, Zhou J, Zhang Y, et al. Insight into biomass pyrolysis mechanism based on cellulose, hemicellulose, and lignin: Evolution of volatiles and kinetics, elucidation of reaction pathways, and characterization of gas, biochar and bio-oil.

- Combust Flame. 2022;242:112142. doi: 10.1016/j.combustflame. 2022.112142.
- [91] Collard FX, Blin J. A review on pyrolysis of biomass constituents: Mechanisms and composition of the products obtained from the conversion of cellulose, hemicellulose, and lignin. Renew Sust Energ Rev. 2014;38:594–608. doi: 10.1016/j.rser.2014.06.013.
- [92] Asmadi M, Kawamoto H, Saka S. Thermal reactions of guaiacol and syringol as lignin model aromatic nuclei. J Anal Appl Pyrolysis. 2011;92(1):88–98. doi: 10.1016/j.jaap.2011.04.011.
- [93] Kawamoto H. Lignin pyrolysis reactions. J Wood Sci. 2017;63:117–32. doi: 10.1007/s10086-016-1606-z.
- [94] Salleh NM, Ismail SA, Ibrahim MN. Radical scavenging activity of lignin extracted from oil palm empty fruit bunch and its effect on glutathione-S-transferase enzymes activity. Asian J Pharm Clin Res. 2015;8(3):81–7.